

Control Orientated Synthesis of High-Performance Piezoelectric Shunt Impedances for Structural Vibration Control

Andrew J. Fleming, *Member, IEEE*, and S. O. Reza Moheimani, *Senior Member, IEEE*

Abstract—Piezoelectric transducers are commonly used as strain actuators in the control of mechanical vibration. One control strategy, termed piezoelectric shunt damping, involves the connection of an electrical impedance to the terminals of a structurally bonded transducer. When subject to deflection, charge generated in the transducer flows through the external impedance developing a counteractive voltage across the terminals. Many passive, nonlinear, and semiactive impedance designs have been proposed that maximize this counteractive effect. This paper introduces a new technique for the design and implementation of piezoelectric shunt impedances. By considering the transducer voltage and charge as inputs and outputs, the design problem is reduced to a standard linear regulator problem enabling the application of standard synthesis techniques such as LQG , \mathcal{H}_2 , and \mathcal{H}_∞ . The resulting impedance is extensible to multitransducer systems, is unrestricted in structure, and is capable of minimizing an arbitrary performance objective. Experimental comparison to a resonant shunt circuit is carried out on a cantilever beam. Previous problems such as *ad hoc* tuning, limited performance, and sensitivity to variation in structural resonance frequencies are significantly alleviated.

Index Terms—Active, damping, noise control, piezoelectric, self-sensing, sensor-less, shunt, vibration.

I. INTRODUCTION

PIEZOELECTRIC TRANSDUCERS have found countless application in such fields as vibration control [1], nano-positioning [2], acoustics [3], and sonar [4]. A piezoelectric transducer undergoes shape transformation when exposed to an electric field and *vice-versa* [4]–[8]. This paper is concerned with the application of piezoelectric transducers in the field of structural noise and vibration control.

In vibration control, piezoelectric transducers are laminated onto the surface of a host structure. As a sensor, the open circuit voltage is proportional to the strain over the region covered by the transducer. As an actuator, an applied voltage results in a moment or transverse force. To model such interaction, the electro-mechanical properties of the transducer are coupled to the mechanical and dynamic response of the structure. A number of methods for deriving such models can be found in [9], [10], and [14]. Consider the typical scenario shown in

Fig. 2, where a flexible structure is excited by a force $f(r, t)$ distributed over the surface. The goal is to suppress resulting vibration measured at a point r . Depending on the application, it may be desirable to minimize displacement, strain, velocity, or acceleration.

Active feedback control involves the use of sensors and actuators to minimize structural vibration. The vibration is sensed directly and used to derive an actuator voltage V_a counteractive to the applied disturbance. Typical vibration sensors include accelerometers, velocimeters, and strain sensors. The foremost difficulties associated with active feedback control are due mainly to the intrinsic nature of the plant G . Mechanical systems are of high order and contain a large number of lightly damped modes. The modeling and control design for such systems is well known to pose significant challenges. In addition, environmental variation of the structural resonance frequencies can further complicate the problem by compromising stability margins and restricting performance. Examples of active feedback control incorporating piezoelectric actuators can be found in [1], [11]–[13].

In active vibration control, and many other applications, piezoelectric transducers are used exclusively as either sensors or actuators. Dosch *et al.* [14] and Anderson *et al.* [15] were able to demonstrate a technique now referred to as piezoelectric self-sensing, or sensor-actuation. By subtracting the capacitive voltage drop from the applied terminal voltage, a reconstruction of the internal piezoelectric strain voltage can be obtained. The reconstructed strain voltage can be employed as an active feedback sensor effectively eliminating the need for an auxiliary transducer. A similar technique estimating the rate-of-strain was also presented in [15]. In addition to the usual problems associated with active feedback control, piezoelectric self-sensing systems are also highly sensitive to the transducer capacitance value. A sensing capacitance not perfectly matched to the transducer capacitance can result in significant errors in the strain estimation. If the estimate is used within a feedback control loop, such uncertainty may severely affect performance or cause instability. An attempt to address the problem of capacitance sensitivity can be found in [16]–[18]. A number of applications utilizing piezoelectric self-sensing actuators have appeared throughout the literature [19]–[23].

Another technique first appearing in [24], termed shunt damping, involves the connection of an electrical impedance to the terminals of a piezoelectric transducer [25]. Impedance designs have included resistors [26], inductive networks [27], [28], switched capacitors [29], switched networks [30], negative

Manuscript received September 2, 2003; revised March 5, 2004. Manuscript received in final form May 5, 2004. Recommended by Associate Editor R. Erwin. This work was supported by the ARC.

The authors are with the School of Electrical Engineering and Computer Science, The University of Newcastle, 2308 Newcastle, Australia (e-mail: andrew@ee.newcastle.edu.au).

Digital Object Identifier 10.1109/TCST.2004.838547

capacitors [31], and active impedances [32]. Shunt damping has a number of benefits and disadvantages when compared to active feedback control. Shunt circuits do not require a feedback sensor, and in some circumstances, may not require any support electronics or power supply at all. Typically, a shunt damping strategy involves a specific impedance structure designed to damp a number of targeted structural modes. Nonlinear optimization approaches have been proposed to automate the design process [33]. Another advantage of shunt damping is that the circuits can be fine-tuned online to compensate for any modeling errors experienced during the design process. Automatic online tuning techniques have also been presented [34].

This paper presents a new framework for the design and implementation of piezoelectric shunt damping circuits. By viewing the transducer voltage and charge as inputs and outputs, the task of impedance design can be cast as a standard regulator problem. Synthesis techniques such as LQG , \mathcal{H}_2 , and \mathcal{H}_∞ can be easily applied to procure a suitable impedance. Unlike present methodologies, the impedance is unrestricted in structure, is multiport for multitransducer systems, and can be designed to meet any performance specification set within the flexibility of the synthesis process.

The following two sections review the basic concepts of impedance synthesis and introduce a simple, charge based modeling technique for piezoelectric laminate structures. Section IV outlines the control objectives and presents LQG , \mathcal{H}_2 , and \mathcal{H}_∞ approaches to the task of impedance synthesis. Experimental results in Section V show superior performance to passive shunt damping circuits. The results and contributions are summarized in Section VI.

II. IMPEDANCE SYNTHESIS

The concept of impedance synthesis for shunt-damping circuits was first presented in [35], [33]. With the use of a voltage controlled current source and signal filter, an arbitrary impedance can be presented to the terminals of a piezoelectric transducer. Synthetic implementation overcomes many previous limitations associated with virtual circuit and direct implementation of piezoelectric shunt damping circuits [33].

As shown in Fig. 1, an electrical impedance $Z(s)$ can also be synthesized with a controlled voltage source, charge measurement, and signal filter. The electric charge $q(t)$, measured in Coulombs (C), is simply the time integral of current. When dealing with capacitive loads, measuring or controlling the charge is convenient as the associated terminal voltage is related proportionally. In contrast, current is related to the terminal voltage through a derivative. If measuring the current and operating over a wide frequency bandwidth, the resulting impedance transfer function is dominated by the derivative and has a correspondingly large dynamic range of at least 20 dB per decade. For practical reasons, it is advantageous to maintain a constant signal level over all frequencies, hence, the motivation for controlling or measuring charge.

To implement a specified impedance $Z(s)$, the terminal voltage V_z , as shown in Fig. 1, should be related to the current i by

$$V_z(s) = Z(s)i(s) \quad (1)$$

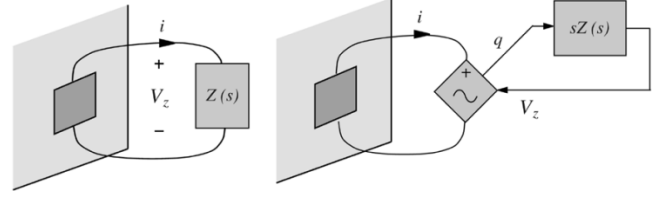


Fig. 1. Impedance synthesis using a charge controlled voltage source.

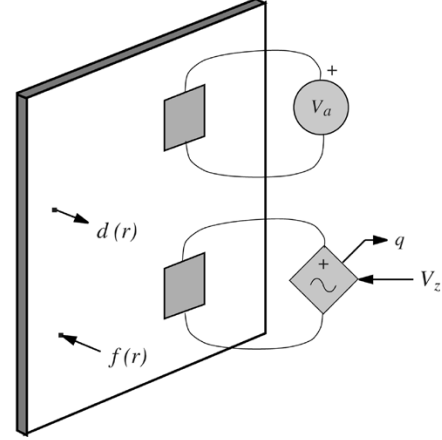


Fig. 2. General piezoelectric laminate structure excited by a distributed force $f(r, t)$ and the voltage $V_a(t)$ applied to a disturbance patch. The resulting vibration $d(r, t)$ is suppressed through the presence of an electrical impedance connected to the shunt transducer.

which implies

$$V_z(s) = sZ(s)q(s). \quad (2)$$

For obvious reasons, the filter $sZ(s)$, will be referred to as an s -impedance.

By viewing the charge q as a measurable system output, and the voltage V_z as an applied control signal, the design of an appropriate s -impedance can be cast as a standard regulator problem. After first modeling the dynamics of a shunted piezoelectric laminate structure in Section III, LQG , \mathcal{H}_∞ , and \mathcal{H}_2 synthesis techniques are applied in Section IV.

III. MODELING

With the aim of facilitating active shunt design, this section introduces a charge-based modeling technique for piezoelectric laminate structures.

Consider the piezoelectric laminate structure shown in Fig. 2. Through the use of a shunt patch driven by the voltage V_z , the goal is to suppress vibration resulting from two disturbances: V_a , the voltage applied to a disturbance patch, and $f(r, t)$ a generally distributed external force. The implemented transfer function between the measured charge q and applied voltage V_z effectively presents an electrical impedance $Z(s)$ to the transducer. The remainder of this section is dedicated to modeling the interaction between structure, transducer, and impedance.

A. Composite Piezoelectric-Mechanical System

Consider the piezoelectric laminate structure shown in Fig. 3(a). The structure is disturbed by m transducers on the left

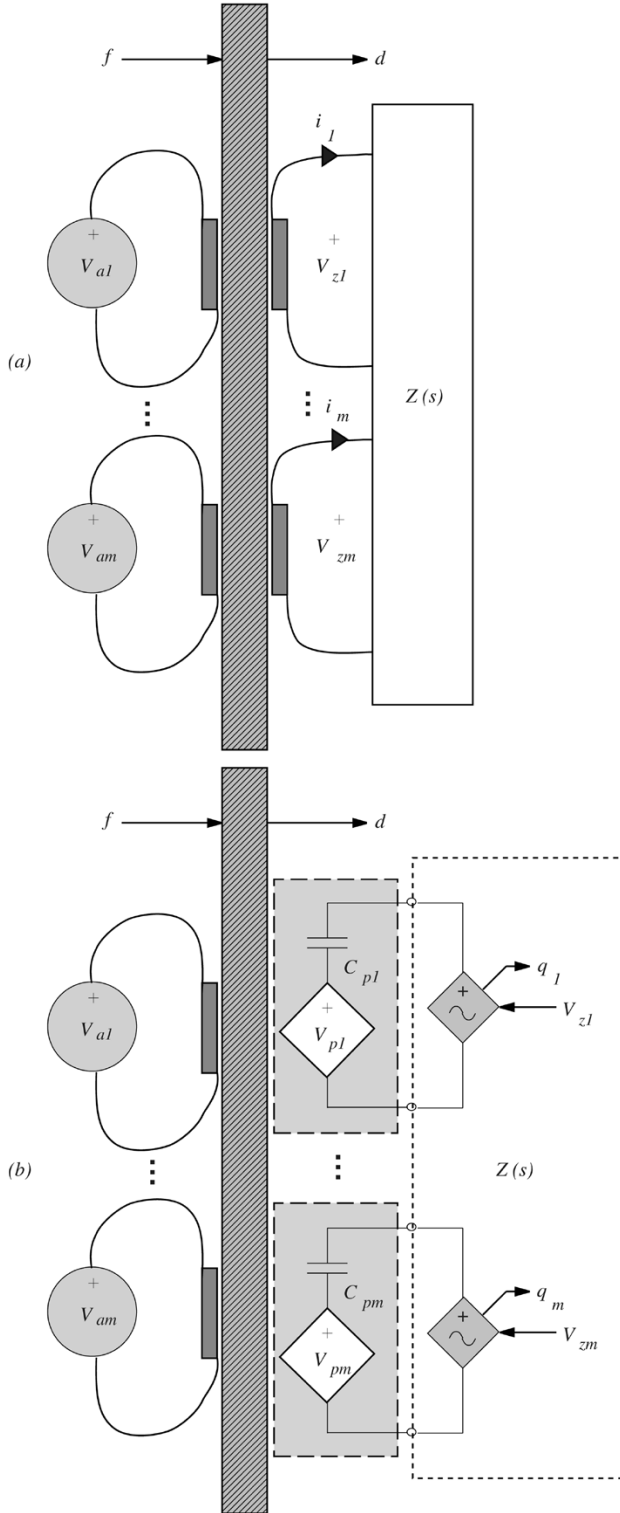


Fig. 3. (a) Shunted multitransducer structure. (b) Synthetic implementation of the impedance.

side, and controlled by a further m collocated transducers on the other. Each piezoelectric transducer is modeled electrically as a capacitor C_{pm} in series with a strain-dependent voltage source v_{pm} [14], [26], [36].

The task of modeling the composite piezoelectric-mechanical system will proceed much as that presented in [37]. The possi-

bility of multiple transducers will be considered. To begin, let us define

$$V_z = \begin{bmatrix} V_{z1} \\ V_{z2} \\ \vdots \\ V_{zm} \end{bmatrix} \quad V_p = \begin{bmatrix} V_{p1} \\ V_{p2} \\ \vdots \\ V_{pm} \end{bmatrix}$$

$$V_a = \begin{bmatrix} V_{a1} \\ V_{a2} \\ \vdots \\ V_{am} \end{bmatrix} \quad i = \begin{bmatrix} i_{z1} \\ i_{z2} \\ \vdots \\ i_{zm} \end{bmatrix}.$$

By applying Ohm's law, and writing Kirchoff's Voltage Law around the k 'th loop, we obtain

$$V_z(s) = Z(s)i(s) \quad (3)$$

$$V_{zk}(s) = V_{pk}(s) - \frac{1}{C_{pk}s}i(s). \quad (4)$$

Assembling the results for each loop

$$V_z(s) = V_p(s) - \frac{1}{s}\Lambda i(s) \quad (5)$$

$$q = -\Lambda^{-1}V_z + \Lambda^{-1}V_p \quad (6)$$

where

$$\Lambda = \begin{bmatrix} \frac{1}{C_{p1}} & & & \\ & \frac{1}{C_{p2}} & & \\ & & \ddots & \\ & & & \frac{1}{C_{pm}} \end{bmatrix}. \quad (7)$$

After applying the principle of superposition, the strain contribution from each disturbance and shunt voltage is

$$V_p(s) = G_{va}(s)V_a(s) + G_{vv}(s)V_z(s) \quad (8)$$

where $G_{va}(s)$ and $G_{vv}(s)$ are the multivariable transfer functions from an applied disturbance and shunt voltage to the piezoelectric voltage V_p , i.e.,

$$G_{va}(s) = \frac{V_p(s)}{V_a(s)} \quad G_{vv}(s) = \frac{V_p(s)}{V_z(s)}. \quad (9)$$

In the case where each disturbance and shunt transducer pair are identical, collocated, and poled in opposite directions, $G_{va}(s) = -G_{vv}(s)$.

Note that this analysis does not require an equal number of disturbance and shunt transducers. This special case is considered only to allow a simplified representation of the feedback diagram associated with the system.

The shunted composite system, alternatively referred to as the closed-loop system, can be obtained from (3), (4), and (8)

$$V_p(s) = \left[I - G_{vv}(s)Z(s) \left(Z(s) + \frac{1}{s}\Lambda \right)^{-1} \right]^{-1} \times G_{va}(s)V_a(s). \quad (10)$$

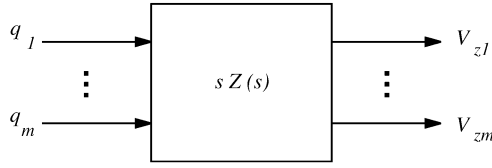


Fig. 4. Multivariable transfer function required to present an impedance $Z(s)$ to the shunt transducers shown in Fig. 3(b).

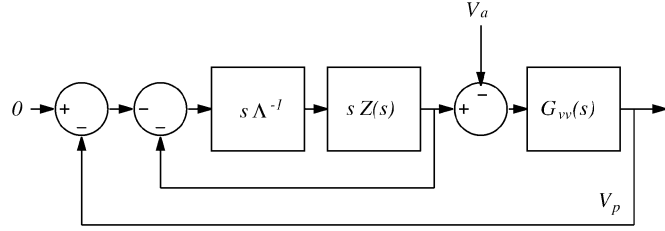


Fig. 5. Equivalent feedback diagram representing (10). In this case, the disturbance and shunt transducers are identical and collocated, i.e., $G_{va}(s) = -G_{vv}(s)$.

In a similar fashion, the composite displacement transfer function can also be derived

$$d(r, s) = \left[I - G_{vv}(s)Z(s) \left(Z(s) + \frac{1}{s}\Lambda \right)^{-1} \right]^{-1} \times G_{da}(s)V_a(s) \quad (11)$$

where $G_{da}(s)$ is the transfer function from an applied disturbance V_a to the resulting displacement d at a point r .

By again applying the principle of superposition, the effect of a generally distributed disturbance force $f(r, s)$ can be included in the composite systems (10) and (11)

$$V_p(s) = \left[I - G_{vv}(s)Z(s) \left(Z(s) + \frac{1}{s}\Lambda \right)^{-1} \right]^{-1} \times (G_{va}(s)V_a(s) + G_{vf}(s)f(s)), \quad (12)$$

$$d(r, s) = \left[I - G_{vv}(s)Z(s) \left(Z(s) + \frac{1}{s}\Lambda \right)^{-1} \right]^{-1} \times (G_{da}(s)V_a(s) + G_{df}(s)f(s)) \quad (13)$$

where $G_{df}(s)$ and $G_{vf}(s)$ are the respective transfer functions from an applied force f to the displacement d and shunt transducer piezoelectric voltage V_p , i.e.,

$$G_{vf}(s) = \frac{V_p(s)}{f(r, s)} \quad G_{df}(s) = \frac{d(r, s)}{f(r, s)}. \quad (14)$$

In [38], the presence of an electrical shunt impedance is viewed as parameterizing an equivalent collocated strain feedback controller. The corresponding multitransducer interpretation is revealed in (10) and (11). In Fig. 5, the multitransducer feedback interpretation is shown to be a direct extension of the single transducer case.

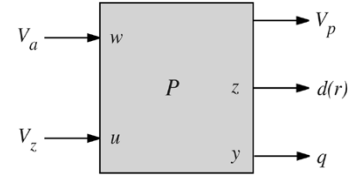


Fig. 6. Composite structural piezoelectric plant P .

Specific models for the transfer functions G_{va} , G_{da} , and G_{vv} will be required throughout the upcoming process of control design. The technique of modal analysis [39], [40] has been used extensively throughout the literature for obtaining structural models. Under certain assumptions [39], the force, transducer voltage, or moment applied to a linear structure can be related to the resulting sensor voltage, strain, or displacement through a transfer function of the following form:

$$G(s) = \sum_{k=1}^{\infty} \frac{\Psi_k}{s^2 + 2\zeta_k\omega_k s + \omega_k^2} \quad (15)$$

where $G(s)$ is intuitively parameterized by the structural resonance frequencies ω_k , modal damping ratios ζ_k , and vector coefficients Ψ_k . In practical applications, where only the first N modes are of importance, the summation is usually truncated accordingly, i.e.,

$$G(s) = \sum_{k=1}^N \frac{\Psi_k}{s^2 + 2\zeta_k\omega_k s + \omega_k^2} + D. \quad (16)$$

The feed-through term D is included to correct in-bandwidth zero locations that are perturbed by the truncation of higher order modes [41]. Based on (16), the system transfer function G_{vv} is defined as

$$G_{vv}(s) = \sum_{k=1}^N \frac{\Psi_k^{vv}}{s^2 + 2\zeta_k\omega_k s + \omega_k^2} + D_{vv}. \quad (17)$$

Likewise for the transfer functions G_{va} , G_{da} , G_{df} , and G_{vf} .

B. Abstracted Plant Model

The general input–output model of a piezoelectric laminate structure is shown in Fig. 6. In conformance with the standard multi-input–multi-output (MIMO) control formulation [42], the plant contains two sets of inputs: the disturbance signals w , and the control signals u . For the case under consideration, the disturbance and control signals are realized through a set of voltages V_a and V_z applied to a number of laminated piezoelectric patches. The system outputs V_p , $d(r)$, and q , correspond, respectively, to the piezoelectric voltages induced in each shunt patch, the dynamic displacement measured at a point r , and the charge resident on each patch. The displacement signal $d(r)$ is chosen as our performance variable z , while the measured charge q is our feedback variable y . Although the induced shunt piezoelectric voltages V_p are not required during the design, their inclusion aids in the modeling process. Given a specific s -impedance, the signal V_p also allows us to compute the equivalent collocated

active feedback controller. A state–space realization of (17) is easily generated to represent the system P

$$\begin{aligned} \dot{x} &= \mathbf{A}x + \mathbf{B} \begin{bmatrix} V_a \\ V_z \end{bmatrix} \\ \begin{bmatrix} V_p \\ d(r) \\ q \end{bmatrix} &= \mathbf{C}x + \mathbf{D} \begin{bmatrix} V_a \\ V_z \end{bmatrix} \end{aligned} \quad (18)$$

where

$$\begin{aligned} \mathbf{A} &= \begin{bmatrix} 0 & 1 & & & & \\ -\omega_1^2 & -2\zeta_1\omega_1 & & & & \\ & & \ddots & & & \\ & & & 0 & 1 & \\ & & & -\omega_N^2 & -2\zeta_N\omega_N^2 & \end{bmatrix} \\ \mathbf{B} = [\mathbf{B}_1 \quad \mathbf{B}_2] &= \begin{bmatrix} 0 & 0 \\ F_1 & H_1 \\ \vdots & \vdots \\ 0 & 0 \\ F_N & H_N \end{bmatrix} \\ \mathbf{C} = \begin{bmatrix} \mathbf{C}_1 \\ \mathbf{C}_2 \\ C_p \mathbf{C}_1 \end{bmatrix} &= \begin{bmatrix} E_1 & 0 & \cdots & E_N & 0 \\ 1 & 0 & \cdots & 1 & 0 \\ C_p E_1 & 0 & \cdots & C_p E_N & 0 \end{bmatrix} \\ \mathbf{D} = \begin{bmatrix} D_{11} & D_{12} \\ D_{21} & D_{22} \\ D_{11}C_p & -C_p + D_{12}C_p \end{bmatrix} \end{aligned} \quad (19)$$

where F_k and H_k $k \in \{1, 2, \dots, N\}$ are the state-input weightings of each disturbance and shunt transducer. The vectors E_k $k \in \{1, 2, \dots, N\}$ represent the contribution of each mode to the induced piezoelectric voltages.

As an alternative to the parameterized modeling approach presented above, a multivariable time or frequency domain system identification technique could be employed to estimate the plant P directly from experimental data [43], [44].

IV. S-IMPEDANCE CONTROL DESIGN

A. LQG Design

Given the composite model discussed in Section III, the problem of designing an appropriate impedance can be cast as a standard regulator problem. As shown in Fig. 7, the regulator $C(s)$ accepts the measured charge q to provide a control signal V_z counteractive to the applied disturbance V_a . The objective is to minimize the structural displacement $d(r)$ subject to a weighting on the magnitude of the required terminal voltage V_z . In a linear quadratic sense, the objective is to minimize

$$J = \int_0^\infty \{d(r, t)^2 + V_z(t)' \mathbf{k}_u V_z(t)\} dt \quad (20)$$

where \mathbf{k}_u is a matrix representing the performance weighting on the applied shunt voltages V_z . Based on the composite plant model (18), the performance signal $d(r, t)$ is represented by

$$d(r, t) = \mathbf{C}_2 x(t) + D_{21} V_a(t) + D_{22} V_z(t). \quad (21)$$

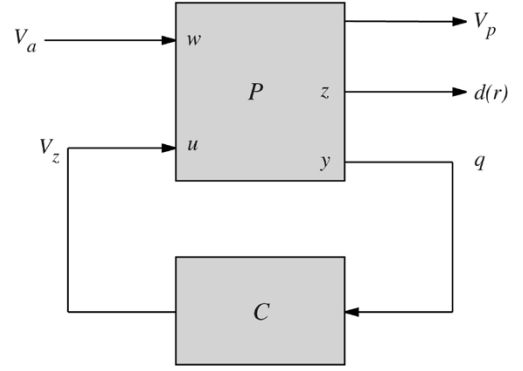


Fig. 7. Composite plant with charge feedback controller $C(s)$.

Considering only the homogeneous component and substituting (21) into (20), the objective function (20) can be rewritten as

$$J = \int_0^\infty \{x'(t) \mathbf{C}'_2 \mathbf{C}_2 x(t) + V_z(t)' D'_{22} D_{22} V_z(t) + 2x'(t) \mathbf{C}'_2 D_{22} V_z(t) + V_z(t)' \mathbf{k}_u V_z(t)\} dt. \quad (22)$$

Restated in the standard LQR context

$$J = \int_0^\infty \{x'(t) \mathbf{Q} x(t) + u(t)' \mathbf{R} u(t) + 2x'(t) \mathbf{N} u(t)\} dt. \quad (23)$$

where

$$\mathbf{Q} = \mathbf{C}'_2 \mathbf{C}_2, \quad \mathbf{R} = D'_{22} D_{22} + \mathbf{k}_u, \quad \mathbf{N} = \mathbf{C}'_2 D_{22}. \quad (24)$$

Through the solution of an algebraic Riccati equation [42], a state feedback matrix K can be found that minimizes the objective function J .

1) *Observer Design:* As the state variables of the system $x(t)$ are not available directly, a linear observer is required.

For s-impedance design, where the controlled plant $(q(s))/(V_z(s))$ is dominated by direct feed-through, the *ad-hoc* pole-placement approach to linear observer design becomes difficult. Although an LQR state-feedback regulator is guaranteed (if \mathbf{R} is chosen diagonal) to result in a phase margin of at least 60° at each plant input channel [45], [46], it is well known that considerable degradation of the stability-margins is to be expected after inclusion of observer dynamics.

A more automated choice in observer design is the Kalman filter [47]. Here, as shown in Fig. 8, the controller $C(s)$ consists of an optimal state-feedback regulator K and Kalman observer O . By the certainty equivalence principle or separation theorem [42], the two entities can be designed independently. After first finding a K to minimize (23), we then design a Kalman filter to minimize

$$J_k = \lim_{t \rightarrow \infty} E\{[x(t) - \tilde{x}(t)][x(t) - \tilde{x}(t)]'\}. \quad (25)$$

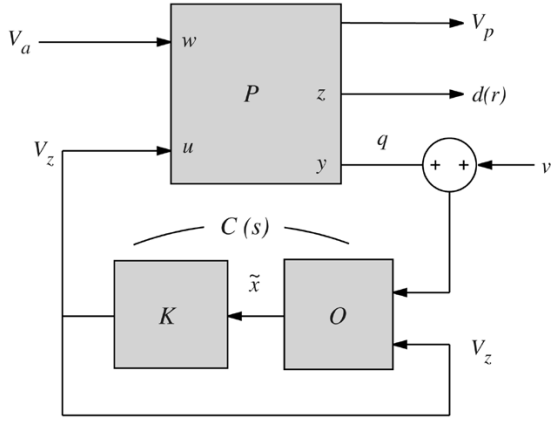


Fig. 8. Composite plant P controlled by $C(s)$, an s -impedance consisting of the optimal state-feedback regulator K , and Kalman filter O .

By the certainty equivalence principle, the optimal K and O also results in minimization of the stochastic performance objective

$$J = E \left\{ \lim_{T \rightarrow \infty} \frac{1}{T} \int_0^T K(t) dt \right\}$$

where $K(t) = x'(t)\mathbf{Q}x(t) + u(t)'\mathbf{R}u(t) + 2x'(t)\mathbf{N}u(t)$. In this scenario, we are referring to the original state-space system (18) with zero-mean uncorrelated Gaussian process models for the disturbance V_a and additive measurement noise v . With the inclusion of measurement noise, the system representation (18) becomes

$$\begin{aligned} \dot{x} &= \mathbf{A}x + \mathbf{B}_1V_a + \mathbf{B}_2V_z \\ \begin{bmatrix} V_p \\ d(r) \\ q \end{bmatrix} &= \mathbf{C}x + \mathbf{D} \begin{bmatrix} V_a \\ V_z \end{bmatrix} + \begin{bmatrix} \mathbf{0} \\ 0 \\ v \end{bmatrix} \end{aligned} \quad (26)$$

where V_a and v satisfy

$$\begin{aligned} E\{V_aV_a'\} &= \mathbf{Q}_n \\ E\{vv'\} &= \mathbf{R}_n. \end{aligned} \quad (27)$$

Based on \mathbf{Q}_n and \mathbf{R}_n , a Kalman observer that minimizes (25) can be found through the solution of an algebraic Riccati equation [42]. The ratio of \mathbf{Q}_n to \mathbf{R}_n essentially represents the confidence in the measured variable q and plant model P . In this work, \mathbf{Q}_n , \mathbf{R}_n , and \mathbf{k}_u , are not quantified and simply treated as design parameters influencing the closed-loop pole locations, damping performance, and closed-loop stability.

B. \mathcal{H}_2 and \mathcal{H}_∞ Design

In contrast to the observer based approaches presented in the previous section, direct output feedback synthesis techniques can also be applied. Fig. 9 illustrates the problem of s -impedance synthesis cast as a standard \mathcal{H}_2 or \mathcal{H}_∞ control problem [48], [49].

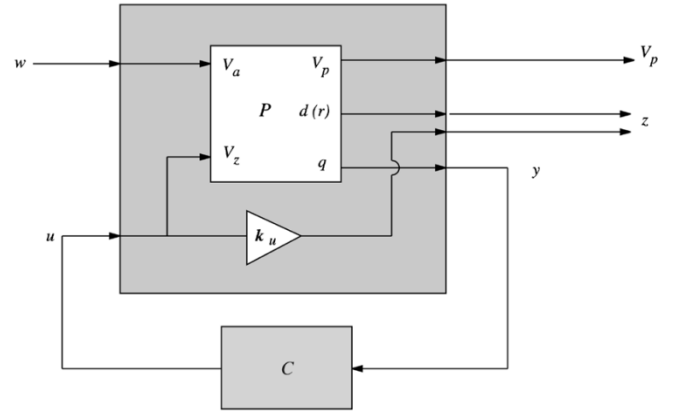


Fig. 9. Standard \mathcal{H}_2 and \mathcal{H}_∞ design problem containing the composite plant P and a secondary performance signal weighting the applied shunt voltage V_z .

In an \mathcal{H}_2 sense, the goal is to minimize the transfer function from an applied disturbance w to the performance signal z , i.e., we seek to minimize

$$\begin{aligned} J &= \left\| \frac{z(s)}{w(s)} \right\|_2 \\ &= \left\| \frac{d(r, s) + \mathbf{k}_uV_z(s)}{V_a(s)} \right\|_2 \end{aligned} \quad (28)$$

where the \mathcal{H}_2 norm $\|F(s)\|_2$ of $F(s)$ is defined as

$$\|F(s)\|_2^2 = \frac{1}{2\pi} \int_{-\infty}^{\infty} \text{tr}\{F(j\omega)F(j\omega)'\} d\omega. \quad (29)$$

By Parseval's equality, the optimal \mathcal{H}_2 controller minimizes the expected root-mean-square (RMS) value of z . An optimal \mathcal{H}_2 controller can be found through the solution of two algebraic Riccati equations [48].

Disadvantages associated with \mathcal{H}_2 and LQG methods include the unrealistic Gaussian disturbance model, and problems related to integral performance constraints [42]. \mathcal{H}_∞ optimization and robust control, originally championed by Zames [50], is an alternative to \mathcal{H}_2 and LQG methods.

Applying \mathcal{H}_∞ control to the problem of s -impedance synthesis involves finding a controller $C(s)$ that minimizes

$$\begin{aligned} J &= \left\| \frac{z(s)}{w(s)} \right\|_\infty \\ &= \left\| \frac{d(r, s) + \mathbf{k}_uV_z(s)}{V_a(s)} \right\|_\infty \end{aligned} \quad (30)$$

where the \mathcal{H}_∞ norm $\|F(s)\|_\infty$ of $F(s)$ is defined as

$$\|F(s)\|_\infty = \max_{\omega} \bar{\sigma}(F(j\omega)) \quad (31)$$

where $\bar{\sigma}$ denotes the maximum singular value.

In the time domain, \mathcal{H}_∞ control can be interpreted as minimizing the worst-case induced 2-norm of z , i.e.,

$$\left\| \frac{z(s)}{w(s)} \right\|_\infty = \max_{w(t) \neq 0} \frac{\|z(t)\|_2}{\|w(t)\|_2} \quad (32)$$

where $\|f(t)\|_2^2 = \int_0^\infty \sum_i |f_i(t)|^2 dt$.

Closely resembling the solution to \mathcal{H}_2 synthesis, an optimal \mathcal{H}_∞ controller can be found through the solution of two algebraic Riccati equations [48].

C. Disturbance Rejection Versus Damping

Before concluding the topic of control synthesis, it is worth comparing our original objectives to that which we have been able to specify within the LQG (20), \mathcal{H}_2 (28), and \mathcal{H}_∞ (30) design frameworks.

The fundamental intention of many active and passive structural control strategies is simply to augment the natural damping inherent in any structure. Using piezoelectric transducers, the only techniques to actually achieve this goal involves full-information state-variable feedback. Measuring selectively and directly the strain, displacement, or velocity of individual modes, requiring the use of distributed modal sensors [51], is a formidable and often deemed impractical approach. More commonly, the controller contains a state-observer designed either explicitly, as in LQR design, or implicitly and possibly internally, as in LQG , \mathcal{H}_2 , and \mathcal{H}_∞ design. The question arises, "Even if the structural poles are moved to a desirable location, what influence do the additional observer dynamics have on the closed-loop system?" Given the spatially distributed nature of the system, an even more fundamental issue is whether a particular design objective results in augmented structural damping (by moving the closed-loop poles), or merely rejection of the represented disturbance. Although rejection of the disturbance w is desirable, in most cases that particular disturbance is only representative, included for the sake of facilitating control design by standard methods. In the case of disturbance rejection, mitigation of a general unmodeled disturbance is not guaranteed. As it occurs in this investigation, both of these issues become especially acute.

First, for LQG design, the desired open- and closed-loop pole locations are shown in Fig. 10. The controller acts to move the lightly damped structural poles further into the complex left-half plane. In addition to the damped structural poles, observer poles, appearing further to the left, are also present. Because of the high degree of damping in these poles, their contribution to the closed-loop system is insignificant. In this scenario, the controller is referred to as augmenting the natural damping of the system. Any applied disturbance encounters a system with heavily damped poles. If a controller exists to arise in such a scenario, through inverse control, the design weights in an LQG problem can be chosen to reproduce it. Unfortunately for conventional choices in the design parameters (24) and (27), the closed-loop pole pattern is likely to present as illustrated in Fig. 11. Even though both scenarios, Figs. 10 and 11, result in identical closed-loop performance, the controller resulting in the second pole pattern is obviously not augmenting the system damping. The residues and, hence,

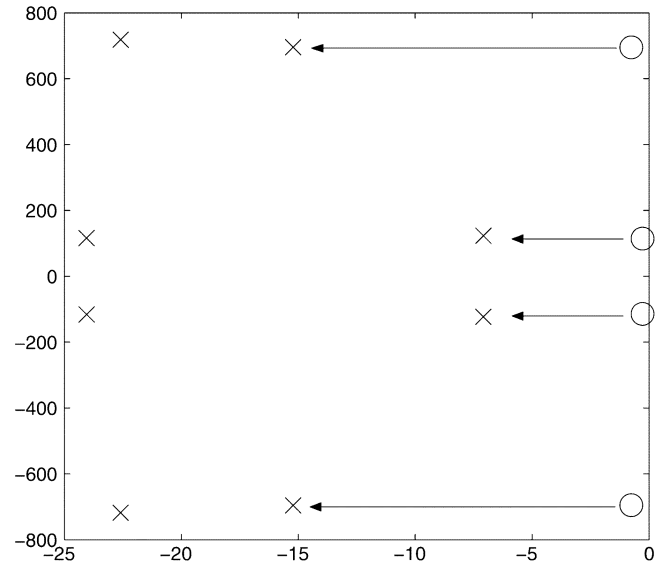


Fig. 10. Pole locations of an open-(O) and closed-loop (x) structural system where the controller augments natural damping.

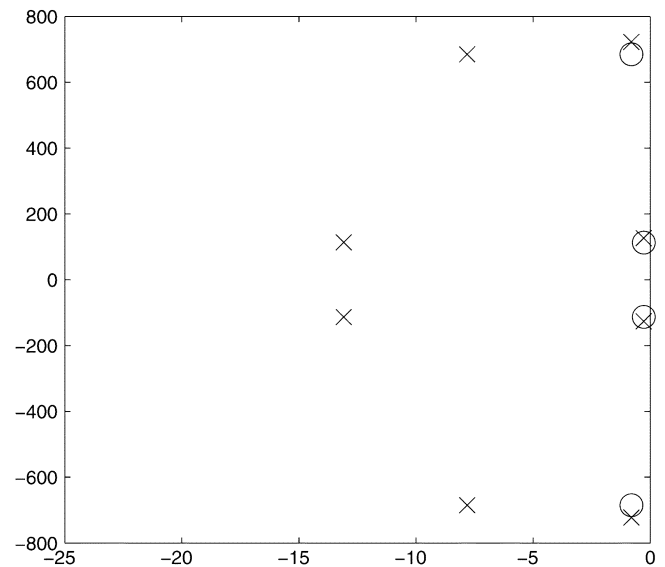


Fig. 11. Pole locations of an open-(O) and closed-loop (x) structural system where the controller does not augment natural damping.

contribution to closed-loop performance, of the lightly damped poles in Fig. 11 are negligible when considering that particular representative disturbance. In the case of disturbances applied through different input channels, the residues of such poles are not insignificant, in fact, they can be disastrous—introducing auxiliary lightly damped resonances and severely degrading performance.

As might be expected due to the similarities in LQG and \mathcal{H}_2 control design, the same situation arises. The performance of an optimal \mathcal{H}_2 controller may be heavily dependent on the disturbance channel. The problem also exists for \mathcal{H}_∞ control.

Being more than just an example, Figs. 10 and 11, are actually the closed-loop pole locations corresponding to two LQG controllers designed for the experimental system introduced in Section V-A. Although both controllers achieve comparable performance, only the first results in augmented system damping.

One can observe that controllers resulting in pole locations resembling Fig. 11, have approximately inverted the open-loop dynamics of the composite plant. During the design we wish to exclude such controllers from the set of all permissible controllers that achieve the specified performance objective. This seemingly complicated restriction can be accomplished in an *ad-hoc* but effective fashion by simply increasing the dimension of the disturbance input w until the plant is no longer square and, hence, uninvertible. The necessary additional disturbance signals should be unique, but are not required to represent a genuine system disturbance. Their inclusion is simply to remove the possibility of plant inversion from the range of outcomes pending control design. In the \mathcal{H}_2 and \mathcal{H}_∞ cases, to avoid distortion of the original performance specification, the influence of such auxiliary disturbances should be chosen small. To a lesser extent, similar care should be taken in the *LQG* case.

For the pole locations shown in Figs. 10 and 11, the corresponding closed-loop *LQG* performance metrics are comparable. The only difference in each problem specification is a small auxiliary input included when designing the controller in Fig. 10. The composite system originally included a single disturbance based on the use of a single shunt patch. The disturbance V_a to the following system was increased in dimension from 1 to 2 by setting $F_k = [F_k \ \alpha_k F_k]$, where α_k is a small random number

$$\begin{aligned} \dot{x} &= \mathbf{A}x + \mathbf{B} \begin{bmatrix} V_a \\ V_z \end{bmatrix} \\ \begin{bmatrix} V_p \\ d(r) \\ q \end{bmatrix} &= \mathbf{C}x + \mathbf{D} \begin{bmatrix} V_a \\ V_z \end{bmatrix} \end{aligned} \quad (33)$$

where

$$\mathbf{B} = [\mathbf{B}_1 \ \mathbf{B}_2] = \begin{bmatrix} 0 & 0 \\ F_1 & H_1 \\ \vdots & \vdots \\ 0 & 0 \\ F_N & H_N \end{bmatrix}. \quad (34)$$

The result is the difference between true system damping and disturbance rejection.

V. EXPERIMENTAL RESULTS

In the following sections, *LQG* and \mathcal{H}_∞ s-impedance controllers are designed and applied experimentally to control a piezoelectric laminate cantilever beam.

A. Experimental Apparatus

The experimental apparatus, shown in Fig. 13 and pictured in Fig. 12, consists of a uniform aluminum cantilever beam. Three piezoelectric transducers are laminated onto the front face and connected electrically in series to the voltage source V_z . A single collocated disturbance transducer, identical to each of the shunt transducers, is also mounted onto the back face and driven with the disturbance voltage V_a . Physical parameters of the beam and piezoelectric transducers can be found in Tables I and II.

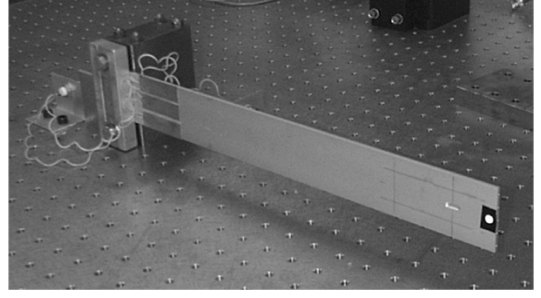


Fig. 12. Cantilever beam.

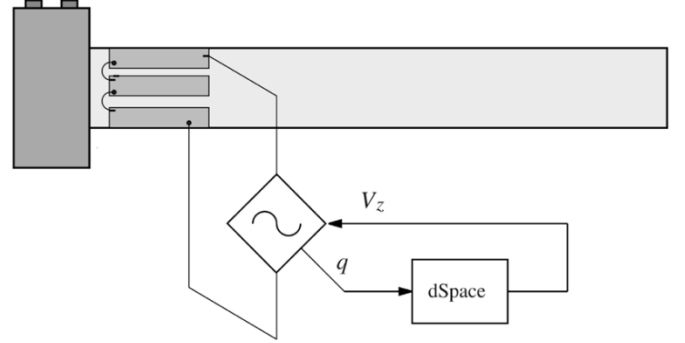


Fig. 13. Front elevation of the cantilever beam. A single co-located disturbance transducer excited by the voltage V_a , is also mounted on the back face.

TABLE I
BEAM PARAMETERS

Length, L	376 mm
Thickness, h	3 mm
Width, W	50 mm
Density, ρ	$2.770 \times 10^3 \text{ kg/m}^3$
Young's Mod., E	$7.00 \times 10^{10} \text{ N/m}^2$

TABLE II
PROPERTIES OF THE PHYSIK INSTRUMENTE TRANSDUCERS (PIC151 CERAMIC)

Length, L_{pz}	50 mm
Thickness, h_{pz}	0.25 mm
Width, W_{pz}	15 mm
Charge Constant, d_{31}	$-210 \times 10^{-12} \text{ m/V}$
Voltage Constant, g_{31}	$-11.5 \times 10^{-3} \text{ Vm/N}$
Coupling Coefficient, k_{31}	0.34
Capacitance, C_p	43 nF
Young's Mod., E_{pz}	$63 \times 10^9 \text{ N/m}^2$

The displacement measurement $d(r, t)$ is acquired using a Polytec PSV300 scanning laser vibrometer.

1) *Voltage Driver With Charge Instrumentation*: The circuit pictured in Fig. 14 is configured to operate as a high-voltage power amplifier with charge instrumentation. As shown in Fig. 15, a high-gain opamp is used to maintain a reference voltage V_{ref} across the load $Z_L(s)$. An arbitrary voltage gain can be implemented by controlling attenuation in the feedback path. The voltage V_s , measured across the sensing capacitor C_s , is proportional to the load charge q . The charge gain in volts per Coulomb is equal to $(1)/(C_s)$, i.e.,

$$\frac{V_s}{q} = \frac{1}{C_s} \frac{V}{C}. \quad (35)$$

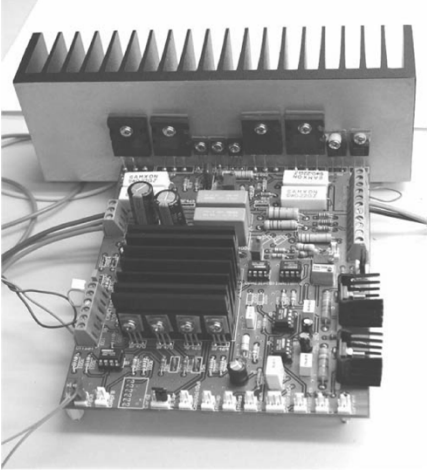


Fig. 14. Implementation of a voltage amplifier with charge instrumentation.

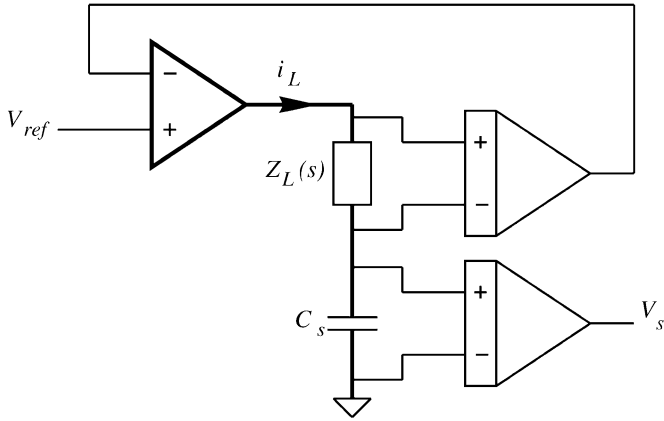


Fig. 15. Voltage amplifier with charge measurement.

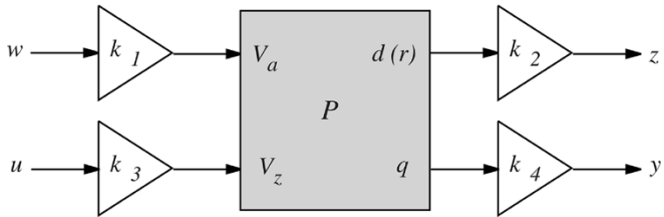


Fig. 16. Composite plant P with external power amplifier and instrumentation gains included.

For implementation of s -impedance controllers, the charge q is defined flowing out of the load, in this case the charge instrumentation gain is negative. An alternative to the circuit shown in Fig. 15 is to interchange the load and sensing impedances. In this case, the feedback voltage is taken directly across the grounded load.

B. Parameter Identification

Before beginning the control design, the parameters of the composite system P must be obtained. As the variables V_a, V_z, q , and $d(r)$ are not driven or accessible directly, the amplifier and instrumentation dynamics will also be included in the model. Shown in Fig. 16, the dynamics encountered through each I/O channel are listed in Table III.

TABLE III
EXPERIMENTAL SYSTEM GAINS

Voltage Gain, k_1	$-10 \frac{V}{V}$
Displacement Gain, k_2	$1 \times 10^3 \frac{V}{m}$
Voltage Gain, k_3	$4 \frac{V}{V}$
Charge Gain, k_4	$\frac{-1}{100 \times 10^9} \frac{V}{C}$

Referring to the system model (18), after inclusion of the amplifier and instrumentation gains, the \mathbf{B} , \mathbf{C} , and \mathbf{D} matrices become

$$\mathbf{B} = [k_1 \mathbf{B}_1 \quad k_3 \mathbf{B}_2] = \begin{bmatrix} 0 & 0 \\ k_1 F_1 & k_3 H_1 \\ \vdots & \vdots \\ 0 & 0 \\ k_1 F_N & k_3 H_N \end{bmatrix} \quad (36)$$

$$\mathbf{C} = \begin{bmatrix} \mathbf{C}_1 \\ k_2 \mathbf{C}_2 \\ k_4 \Lambda^{-1} \mathbf{C}_1 \end{bmatrix} = \begin{bmatrix} E_1 & 0 & \cdots & E_N & 0 \\ k_2 & 0 & \cdots & k_2 & 0 \\ \Lambda^{-1} k_4 E_1 & 0 & \cdots & \Lambda^{-1} k_4 E_N & 0 \end{bmatrix} \quad (37)$$

$$\mathbf{D} = \begin{bmatrix} D_{11} & D_{12} \\ k_1 k_2 D_{21} & k_3 k_2 D_{22} \\ k_1 k_4 D_{11} \Lambda^{-1} & k_3 k_4 [-\Lambda^{-1} + D_{12} \Lambda^{-1}] \end{bmatrix}. \quad (38)$$

To determine the model parameters, a simple optimization scheme is employed. From an initial guess, ω_i and ς_i , are found through a simplex optimization based on the frequency response from an applied disturbance to the measured displacement

$$[\omega_k \quad \varsigma_k] = \arg \min \left\| \tilde{P}_{dV_a}(j\omega) - P_{dV_a}(j\omega) \right\|_2 \quad (39)$$

where $\tilde{P}_{dV_a}(j\omega)$ is the measured frequency response from an applied disturbance $V_a(s)$ to the displacement $d(r, s)$. With these parameters in hand, those remaining are determined from a final global optimization

$$\arg \min \| \tilde{P}(j\omega) - P(j\omega) \|_{2, W}. \quad (40)$$

As gains from channel to channel vary greatly, a multivariable frequency weight W is required to normalize the cost of each error transfer function.

The magnitude and phase response of the measured system and resulting model are shown in Figs. 17 and 18. The model is an accurate representation of the measured system. Note the close pole-zero spacing in the transfer function from an applied shunt voltage V_z to the charge q . Referring to (19), this behavior is due to the transducer capacitance which results in a large direct feed-through.

In the following sections, it will be of interest to examine the robustness of each control strategy subject to a change in the structural resonance frequencies. Experimentally, such variation is accomplished by affixing a mass 60 mm from the beam tip. The corresponding change in structural resonance frequencies is illustrated in Fig. 20.

C. Passive Shunt Design

For the sake of comparison, each LQG and \mathcal{H}_∞ shunt impedance will be judged against a traditional resonant piezo-

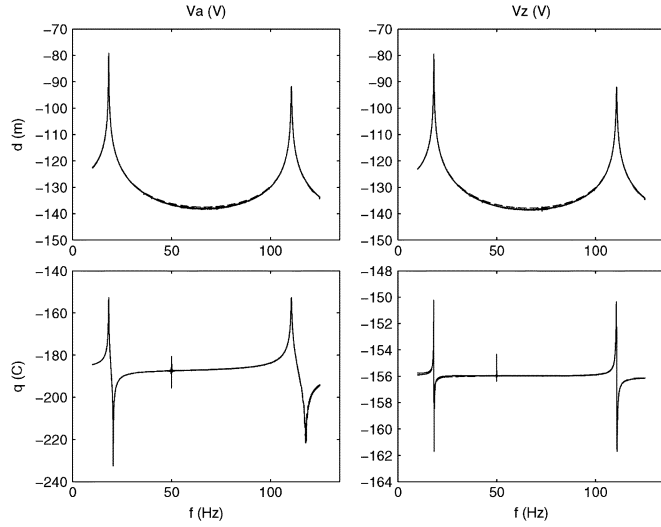


Fig. 17. Simulated (---) and experimental (—) magnitude frequency response of the shunt voltage controlled piezoelectric beam (in decibels).

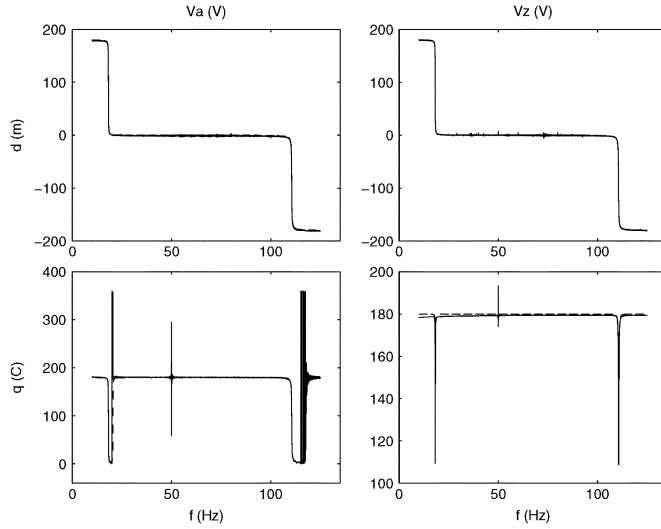


Fig. 18. Simulated (---) and experimental (—) phase frequency response of the shunt voltage controlled piezoelectric beam (in degrees).

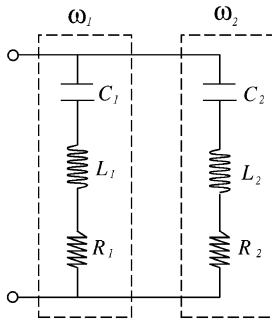


Fig. 19. Dual-mode current-flowing piezoelectric shunt damping circuit [52].

electric shunt damping circuit applied to the same structure. A current-flowing shunt circuit [52] was designed and tuned to minimize the \mathcal{H}_2 norm of the cantilever beam. The schematic and component values can be found in Fig. 19 and Table IV.

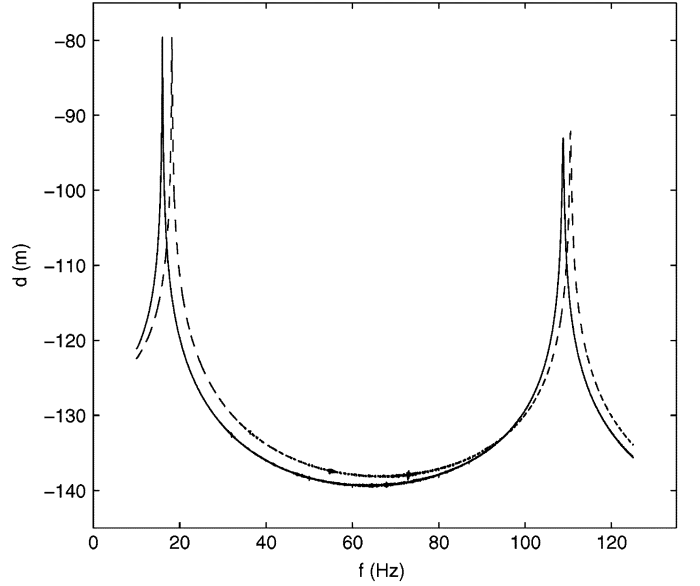


Fig. 20. Experimental frequency response (in decibels) from an applied disturbance voltage $V_a(V)$ to the resulting tip displacement $d(m)$. Free (---), with Mass (—).

TABLE IV
COMPONENT VALUES OF THE CURRENT-FLOWING SHUNT CIRCUIT

C_1	10 nF	C_2	10 nF
L_1	11690 H	L_2	348 H
R_1	15 k Ω	R_2	9 k Ω

D. LQG Shunt Design

Following the procedure described in Section IV-A, an s -impedance can be designed and implemented to minimize an LQG performance objective. Based on the state-space model procured in Section V-B, an LQR gain matrix was designed to minimize the following cost function:

$$J = \int_0^{\infty} \{d(r, t)^2 + k_u V_z(t)^2\} dt \quad (41)$$

where k_u , the control signal weighting, was chosen to be 2.6×10^{-11} . Considering the relative difference in magnitude between the displacement $d(r, t)$ and $V_z(t)$, a small value for k_u is not unexpected.

With the addition of an auxiliary input to avoid plant inversion, a Kalman observer was designed to estimate the system state $x(t)$ utilizing the measured shunt transducer charge $q(t)$ and control signal $V_z(t)$. Referring to Section IV-A, the disturbance and output noise process covariance matrices, \mathbf{Q}_n and \mathbf{R}_n , were chosen as 1 and 0.1, respectively. Such a weighting, although not quantitative, expresses a moderate confidence in the fidelity of the measured variable q .

By concatenating the LQR gain matrix and Kalman observer, and compensating for the system gains k_3 and k_4 , the actual impedance presented to the shunt transducer can be determined. In Fig. 21, the complex s -impedance of the resulting controller is plotted together with the s -impedance of an ideal negative capacitor controller [32], [31]. The LQG controller mimics the response of an ideal negative capacitor at frequencies in the

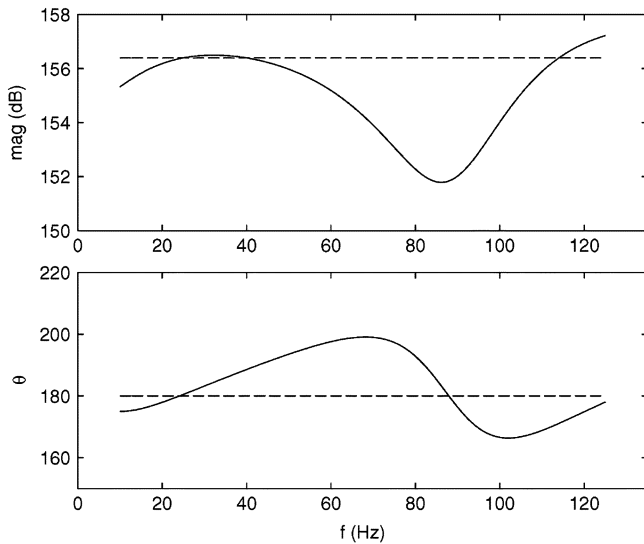


Fig. 21. Complex s -impedance of the LQG (—), and ideal negative capacitor (---) shunt controller.

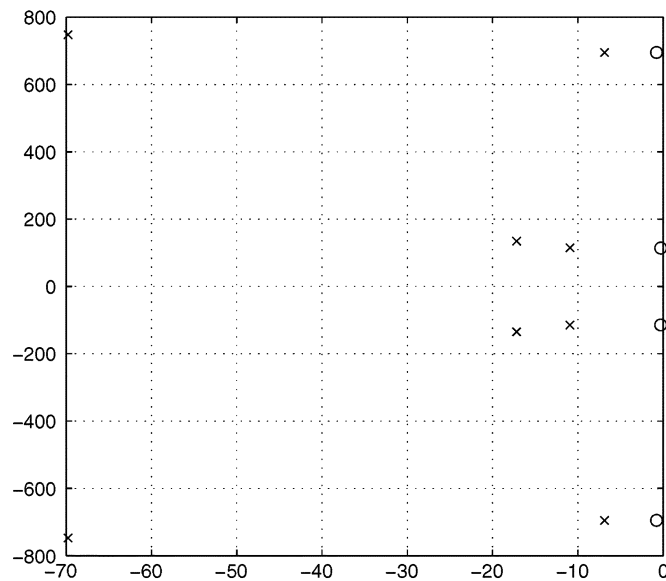


Fig. 22. Open-(O), and closed-loop (x) pole locations of the LQG shunt controlled system.

vicinity of each structural resonance. Unlike the negative capacitor which is equivalent to applying an infinite feedback gain over all frequencies, the LQG controller exerts influence only where necessary and has the benefit of rolling off at higher frequencies.

After examining the open- and closed-loop pole locations shown in Fig. 22, it can be concluded that the controller is clearly acting to increase the system damping. Corresponding mitigation of the transfer function from an applied disturbance to the measured displacement can be seen in both the frequency domain, Fig. 23, and time domain, Fig. 25. The magnitudes of the first and second structural modes are reduced by 27.2 and 19.2 dB, respectively. As the second mode contributes significantly less to the LQG cost function, the majority of control effort is expended on the first and most dominant mode. The

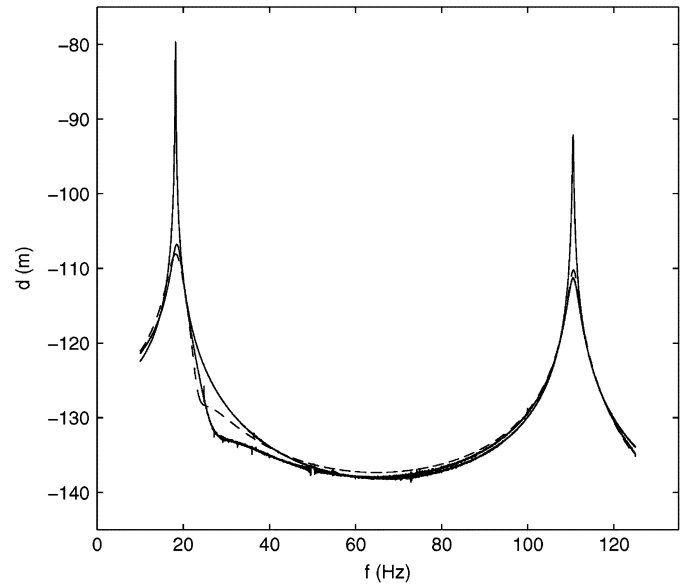


Fig. 23. Experimental (—), and simulated (---), LQG shunt controlled frequency responses from an applied disturbance voltage $V_a(V)$ to the resulting tip displacement $d(m)$ (in decibels). The open-loop frequency response is also shown (—).

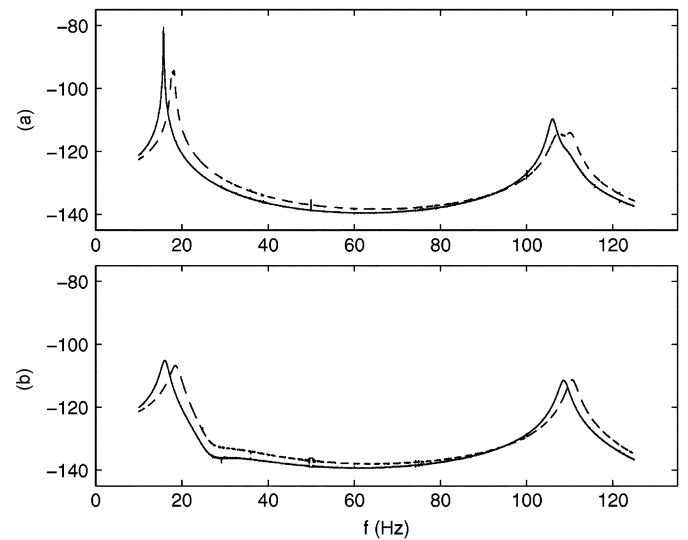


Fig. 24. Free (---), and with-mass (—). (a) Passive. (b) LQG shunt controlled experimental frequency responses from an applied disturbance voltage $V_a(V)$ to the resulting tip displacement $d(m)$ (in decibels).

damping ratios of the first and second structural modes are increased from 0.002 46 to 0.0948, and from 0.0011 to 0.009 89.

An unexpected feature of the LQG s -impedance is its smooth frequency response; there are no localized peaks at the resonance frequencies. In contrast, high-performance active strain-, velocity-, and acceleration-feedback controllers characteristically apply a highly localized gain at the frequencies of structural resonance. In the advent of model variation, such localized behavior can result in considerable performance degradation. In order to examine system robustness, the nominal system is perturbed by adding a mass 60 mm from the beam tip. Aside from the disturbance to the underlying partial differential equation, the first and second resonance frequencies are decreased by 13.5 and 2.2%, respectively. The consequence on both passive and

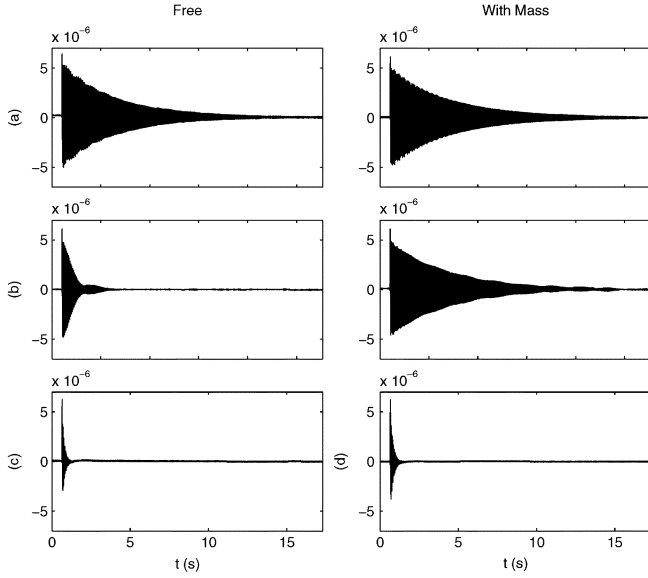


Fig. 25. Free (left column) and with-mass (right column) tip displacement response $d(m)$ to a step disturbance in V_a . (a) Experimental open-loop. (b) Passive shunt controlled. (c) LQG shunt controlled systems.

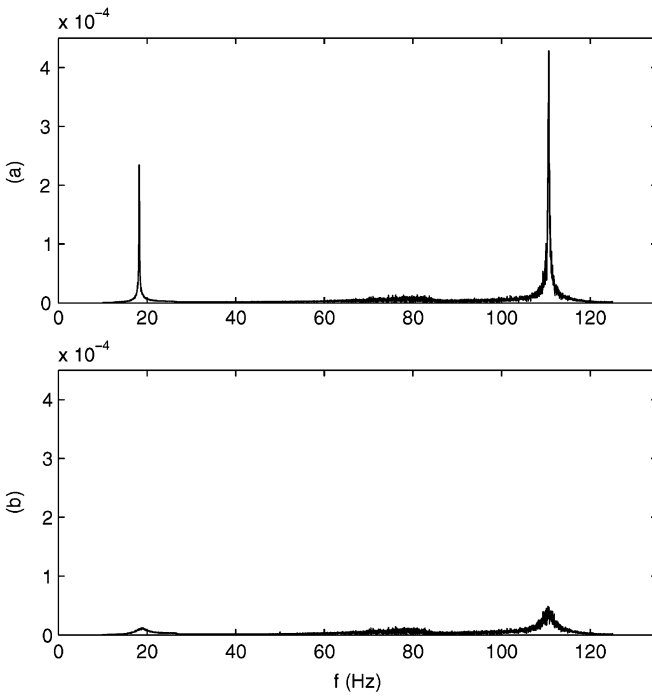


Fig. 26. (a) Open-loop and (b) LQG shunt controlled linear magnitude response from an applied acoustic disturbance to the resulting tip displacement $d(m)$.

active shunt circuits is shown in Fig. 24. While the LQG shunt loses only 1.7 and 0.2 dB from its unperturbed attenuation of the first and second modes, the passive shunt loses 13.4 and 4.8 dB. Corresponding time domain results are shown in Fig. 25.

In a final test to validate the LQG s -impedance, an acoustic loud speaker was used to spatially excite the structure. The measured frequency response, shown in Fig. 26, verifies that the achieved performance is disturbance-channel independent.

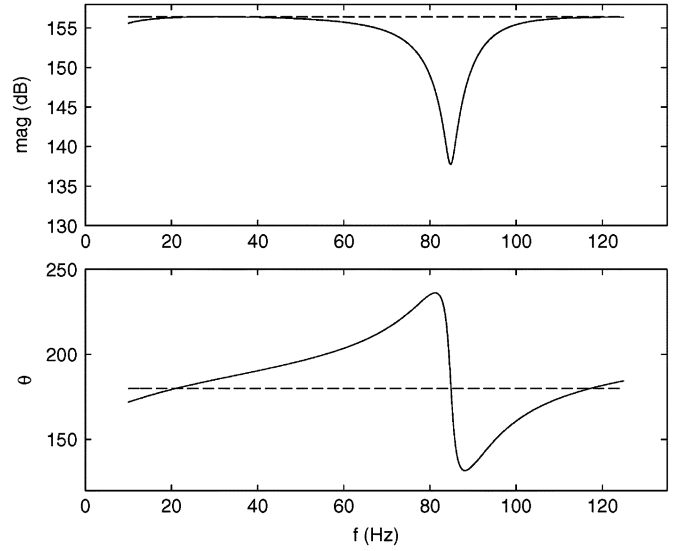


Fig. 27. Complex s -impedance of the \mathcal{H}_∞ (—), and ideal negative capacitor (---) shunt controller.

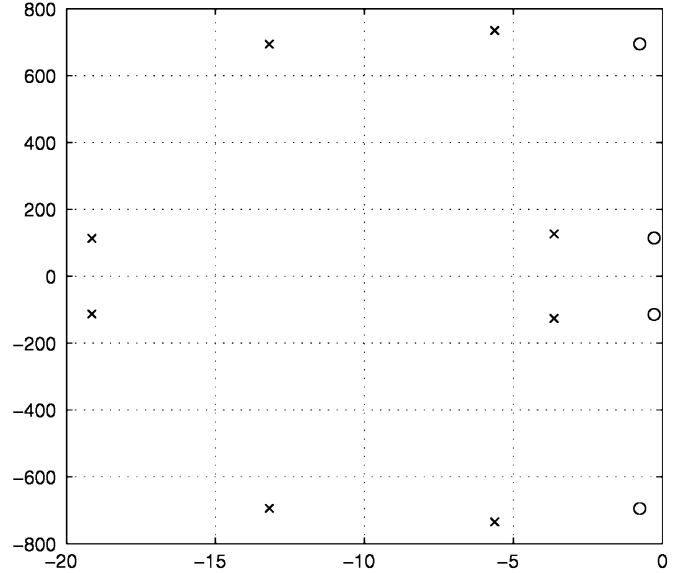


Fig. 28. Open-(O), and closed-loop (x) pole locations of the \mathcal{H}_∞ shunt controlled system.

E. \mathcal{H}_∞ Shunt Design

This section documents the design and implementation of an \mathcal{H}_∞ s -impedance. As discussed in Section IV-B, an \mathcal{H}_∞ s -impedance is designed to minimize the following cost function:

$$J = \left\| \left\| \frac{d(r, s) + k_u V_z(s)}{V_a(s)} \right\| \right\|_\infty \quad (42)$$

where k_u , the control signal weighting, was chosen to be 3.2×10^{-7} . A random auxiliary input of negligible influence was also included to avoid plant inversion.

The complex s -impedance of the resulting \mathcal{H}_∞ controller is plotted in Fig. 27.

Examining the open- and closed-loop pole locations shown in Fig. 28, the controller is clearly augmenting the system damping. Corresponding mitigation of the transfer function

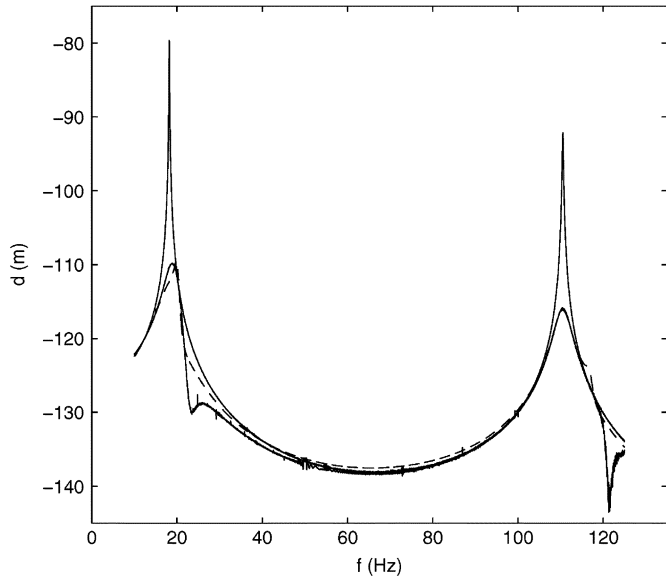


Fig. 29. Experimental (—), and simulated (---), \mathcal{H}_∞ shunt controlled frequency responses from an applied disturbance voltage $V_a(V)$ to the resulting tip displacement $d(m)$ (in decibels). The open-loop response is also shown (—).

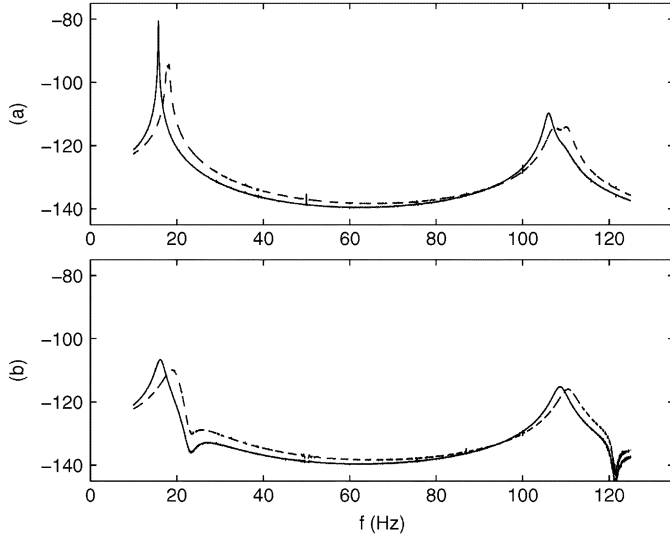


Fig. 30. Free (---), and with-mass (—). (a) Passive and \mathcal{H}_∞ (b) shunt controlled experimental frequency responses from an applied disturbance voltage $V_a(V)$ to the resulting tip displacement $d(m)$ (in decibels).

from an applied disturbance to the measured displacement can be seen in both the frequency domain, Fig. 29, and time domain, Fig. 31. The magnitudes of the first and second structural modes are reduced by 30.3 and 24.0 dB, respectively. Damping ratios are increased from 0.00246 to 0.0288, and from 0.0011 to 0.00766.

The effect of additional mass can be observed in Figs. 30 and 31. The \mathcal{H}_∞ controller loses 3.3 and 0.8 dB from its nominal closed-loop attenuation of the first and second modes.

Acoustic excitation results in both the frequency and time domains are shown in Figs. 33 and 32.

VI. CONCLUSION

A framework has been presented for the design of active shunt impedances. By viewing a piezoelectric laminate structure as a

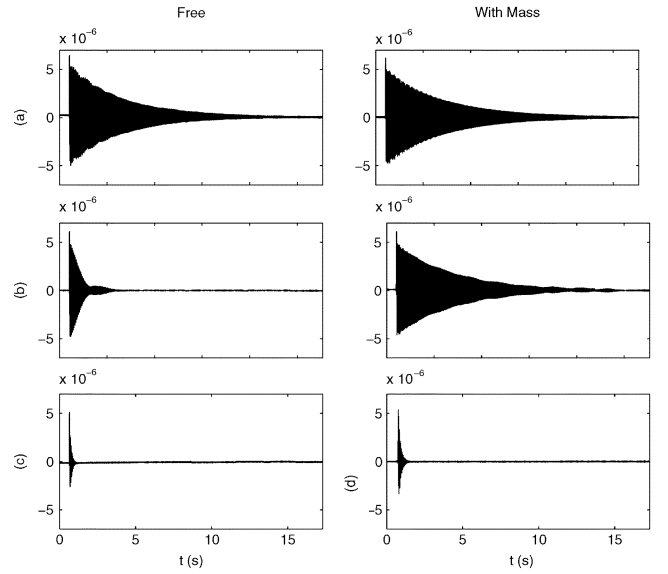


Fig. 31. Free (left column) and with-mass (right column) tip displacement response $d(m)$ to a step disturbance in V_a . (a) Experimental open-loop. (b) Passive shunt controlled. (c) \mathcal{H}_∞ shunt controlled systems.

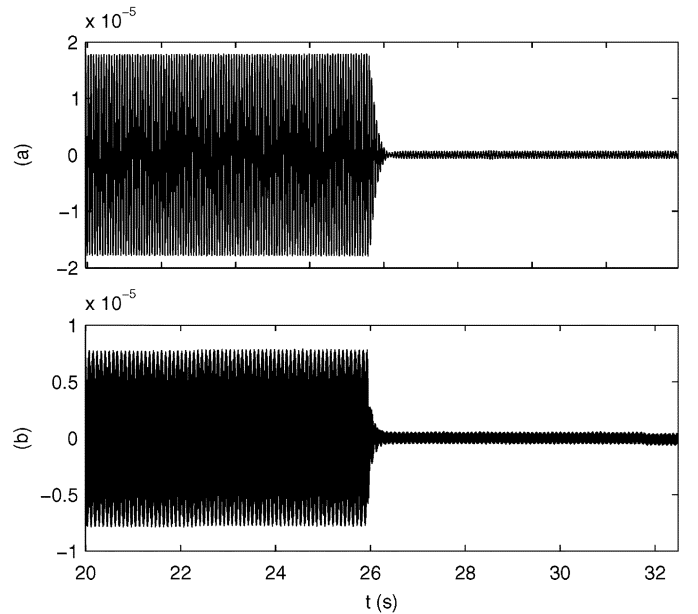


Fig. 32. Open-loop and \mathcal{H}_∞ shunt controlled tip displacement response $d(m)$ to an acoustic sinusoidal disturbance at the (a) first and (b) second structural resonance frequencies. Control is applied at approximately time 25.8 s.

system with transducer voltage inputs and charge outputs, the task of shunt impedance design can be accomplished through the solution of a standard control problem, e.g., by LQG , \mathcal{H}_2 , or \mathcal{H}_∞ synthesis. The resulting controller, effectively the derivative of impedance, can be implemented directly with a voltage amplifier and charge measurement.

Although the fundamental goal in smart structure design is often to augment system damping, this cannot be specified directly as an LQG , \mathcal{H}_2 , or \mathcal{H}_∞ performance objectives. The approach has been to achieve this indirectly through mitigation of the performance transfer function $(d(s))/(V_a(s))$.

As the system we are considering is spatially distributed, our controller should ensure performance subject to any realizable

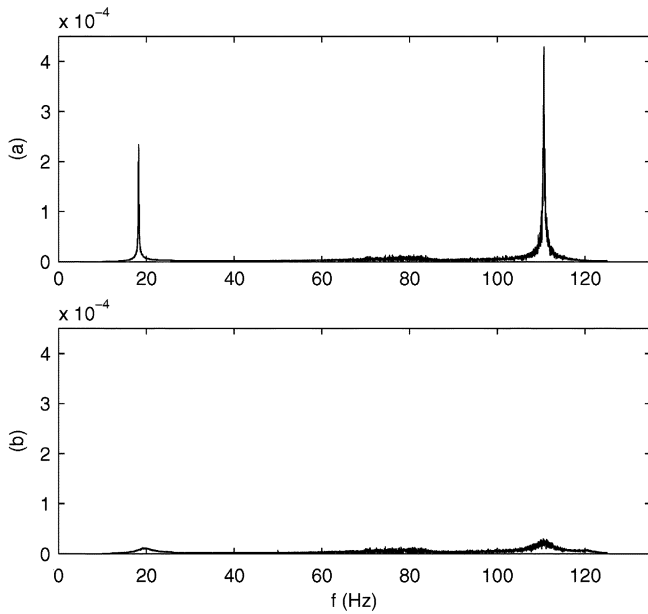


Fig. 33.(a) Open-loop and (b) \mathcal{H}_∞ shunt controlled linear magnitude response from an applied acoustic disturbance to the resulting tip displacement $d(m)$.

TABLE V
MAGNITUDE ATTENUATION SUMMARY

Frequency	1 st Mode		2 nd Mode	
	Unperturbed	Perturbed	Unperturbed	Perturbed
Passive	14.2 dB	0.8 dB	22.1 dB	17.3 dB
LQG	27.2 dB	25.5 dB	19.2 dB	19.4 dB
\mathcal{H}_∞	30.3 dB	27.0 dB	24.0 dB	23.2 dB

disturbance. To achieve this, an *ad-hoc* technique has been proposed to avoid the possibility of disturbance channel sensitivity and plant inversion.

Experimentally, the active shunts have proven to introduce significant system damping, up to 30.3 dB attenuation of the first cantilever mode. A comparison of modal attenuation for each active shunt impedance can be found in Table V. The performance of a current-flowing passive shunt circuit is included as a reference.

While achieving levels of performance previously only available through sensor-based feedback control, active shunt impedances are remarkably insensitive to variation in the structural resonance frequencies. A 13.5% change in the first resonance frequency resulted in only a slight loss in performance. By comparison, the same variation had a disastrous consequence on the performance of a passive shunt damping circuit. Such sensitivity has previously limited the practical application of active and passive vibration control systems in smart structure design.

Another well known problem associated with passive shunt damping is the lack of control influence. Given a lightly damped structure, even the small counteractive forces associated with passive shunt circuits can significantly increase system damping. Many practical mechanical structures naturally exhibit higher levels of damping. In such cases, passive piezoelectric shunt circuits are of limited use. As the amount of control influence associated with active shunt impedances is arbitrary, the possibility now exists for controlling more heavily damped systems. In such cases, the control voltage V_z is expected to become quite large.

At high-drive voltages it may become necessary to address the inherent piezoelectric hysteresis.

The reader will appreciate that the presented techniques are quite general and valid for structures incorporating multiple piezoelectric transducers. Although the application of sensor-based feedback control is well defined and feasible for structures with multiple sensors and actuators, the same can not be said for multitransducer shunt circuits [37]. Present multitransducer, multimode shunt circuits are simply a direct extension of single transducer shunt circuits. Each circuit is restricted to be independent and attached to a single transducer. If a single mode is to be targeted by two or more transducers, the task of tuning the shunt circuit can become extremely tedious. In addition to the complicated interaction between transducers at those frequencies, there are now as many more tuning parameters as there are transducers per mode. The design freedom afforded with active shunts not only eliminates the complicated task of tuning, but allows for full utilization of each patch. The resulting impedance is unstructured, multivariable, and able to exploit benefits that may arise from inter-transducer coupling.

Potential applications for active piezoelectric shunt control include sensor-less, high-performance vibration control of acoustic panels, flexible structures, and positioning systems. Future work includes multitransducer structures and passive impedance design. The LQG , and \mathcal{H}_∞ impedances contained negative reactive components and are unstable in a systems perspective. Although the connection of the transducer and control impedance is stable, an inherently stable controller is desirable. It is presently unclear if negative reactive components are necessary to result in effective vibration reduction. (Impedance pole-zero maps can be found in [53]).

REFERENCES

- [1] N. W. Hagood, W. H. Chung, and A. von Flotow, "Modeling of piezoelectric actuator dynamics for active structural control," *J. Intell. Material Syst. Structures*, vol. 1, pp. 327–354, 1990.
- [2] C. Niezrecki and H. H. Cudney, "Feasibility to control launch vehicle internal acoustics using piezoelectric actuators," *J. Intell. Material Syst. Structures*, vol. 12, pp. 647–660, Sep. 2001.
- [3] D. Stansfield, *Underwater Electroacoustic Transducers*, Bath, U.K.: Bath Univ. Press, 1991.
- [4] C. R. Fuller, S. J. Elliott, and P. A. Nelson, *Active Control of Vibration*. New York: Academic, 1996.
- [5] B. Jaffe, W. R. Cook, and H. Jaffe, *Piezoelectric Ceramics*. New York: Academic, 1971.
- [6] H. Janocha, *Adaptronics and Smart Structures—Basics, Material, Design, and Applications*. New York: Springer-Verlag, 1999.
- [7] *IEEE Standard on Piezoelectricity*, ANSI/IEEE Standard 176, 1987.
- [8] H. J. M. T. A. Adriaens, W. L. de Koning, and R. Banning, "Modeling piezoelectric actuators," *IEEE/ASME Trans. Mechatron.*, vol. 5, no. 4, pp. 331–341, Dec. 2000.
- [9] T. E. Alberts and J. A. Colvin, "Observations on the nature of transfer functions for control of piezoelectric laminates," *J. Intell. Material Syst. Structures*, vol. 8, no. 5, pp. 605–611, 1991.
- [10] R. L. Clark, W. R. Saunders, and G. P. Gibbs, *Adaptive Structures: Dynamics and Control*. New York: Wiley, 1998.
- [11] E. Garcia, J. D. Dosch, and D. J. Inman, "Vibration attenuation in an active antenna structure," in *Proc. Conf. Recent Advances in Active Control of Sound and Vibration*. Blacksburg, VA, Apr. 15–17, 1991, pp. S35–S42.
- [12] E. Garcia, D. J. Inman, and J. D. Dosch, "Vibration suppression using smart structures," *Proc. SPIE Smart Structures Materials*, pp. 167–172, 1991.
- [13] K. B. Lazarus and E. F. Crawley, "Multivariable active lifting surface control using strain actuation: Analytical and experimental results," in *Proc. 3rd Int. Conf. Adaptive Structures*, San Diego, CA, 1992, pp. 87–101.

- [14] J. J. Dosch, D. J. Inman, and E. Garcia, "A self-sensing piezoelectric actuator for collocated control," *J. Intell. Material Syst. Structures*, vol. 3, pp. 166–185, Jan. 1992.
- [15] E. H. Anderson, N. W. Hagood, and J. M. Goodliffe, "Self-sensing piezoelectric actuation: Analysis and application to controlled structures," in *Proc. AIAA/ASME/ASCE/AHS/ASC Structures, Structural Dynamics, and Materials*, 1992, pp. 2141–2155.
- [16] J. S. Vipperman and R. L. Clark, "Hybrid analog and digital adaptive compensation of piezoelectric sensor/actuators," in *Proc. AIAA/ASME Adaptive Structures Forum*, New Orleans, LA, 1995, pp. 2854–2859.
- [17] D. G. Cole and R. L. Clark, "Adaptive compensation of piezoelectric sensor/actuators," *J. Intell. Material Syst. Structures*, vol. 5, pp. 665–672, 1994.
- [18] S. Acrabelli and A. Tonoli, "System properties of flexible structures with self-sensing piezoelectric transducers," *J. Sound Vib.*, vol. 235, no. 1, pp. 1–23, 2000.
- [19] J. B. Aldrich, N. W. Hagood, A. von Flotow, and D. W. Vos, "Design of passive piezoelectric shunt damping for space structures," in *Proc. SPIE Conf. Smart Structures and Intelligent Systems*, vol. 1917, 1993, pp. 629–705.
- [20] E. Bianchini, R. Spangler, and C. Andrus, "The use of piezoelectric devices to control snowboard vibrations," in *Proc. SPIE Smart Structures and Materials: Smart Structures and Integrated Systems*, vol. 3329, 1998, pp. 106–114.
- [21] N. W. Hagood and E. F. Crawley, "Experimental investigation of passive enhancement of damping for space structures," *J. Guid. Control Dyn.*, vol. 14, no. 6, pp. 1100–1109, 1991.
- [22] S. Kim, C. Han, and C. Yun, "Improvement of aeroelastic stability of hingeless helicopter rotor blade by passive piezoelectric damping," in *Proc. SPIE Smart Structures and Materials: Passive Damping and Isolation*, vol. 3672, Newport Beach, CA, Mar. 1999, pp. 131–141.
- [23] P. Vallone, "High-performance piezo-based self-sensor for structural vibration control," in *Proc. SPIE Smart Structures and Materials: Smart Structures and Integrated Systems*, vol. 2443, 1995, pp. 643–655.
- [24] R. L. Forward, "Electronic damping of vibrations in optical structures," *Appl. Opt.*, vol. 18, no. 5, pp. 690–697, Mar. 1979.
- [25] S. O. R. Moheimani, "A survey of recent innovations in vibration damping and control using shunted piezoelectric transducers," *IEEE Trans. Contr. Syst. Technol.*, vol. 11, no. 4, pp. 482–494, Jul. 2003.
- [26] N. W. Hagood and A. Von Flotow, "Damping of structural vibrations with piezoelectric materials and passive electrical networks," *J. Sound Vib.*, vol. 146, no. 2, pp. 243–268, 1991.
- [27] S. Y. Wu and A. S. Bicos, "Structural vibration damping experiments using improved piezoelectric shunts," in *Proc. SPIE Smart Structures and Materials, Passive Damping and Isolation*, vol. 3045, Mar. 1997, pp. 40–50.
- [28] S. Behrens, S. O. R. Moheimani, and A. J. Fleming, "Multiple mode passive piezoelectric shunt dampener," in *Proc. IFAC Mechatronics*, Berkeley, CA, Dec. 2002.
- [29] L. R. Corr and W. W. Clark, "Comparison of low-frequency piezoelectric switching shunt techniques for structural damping," *IOP Smart Materials and Structures*, vol. 11, pp. 370–376, 2002.
- [30] C. Richard, D. Guyomar, D. Audigier, and H. Bassaler, "Enhanced semi-passive damping using continuous switching of a piezoelectric devices on an inductor," in *Proc. SPIE Smart Structures and Materials, Damping and Isolation*, vol. 3989, Newport Beach, CA, Mar. 2000, pp. 288–299.
- [31] S. Y. Wu, "Broadband piezoelectric shunts for structural vibration control," Patent no. 6075309, Jun. 2000.
- [32] S. Behrens, A. J. Fleming, and S. O. R. Moheimani, "A broadband controller for piezoelectric shunt damping of structural vibration," *IOP Smart Materials and Structures*, vol. 12, pp. 18–28, Jan. 2003.
- [33] A. J. Fleming, S. Behrens, and S. O. R. Moheimani, "Optimization and implementation of multi-mode piezoelectric shunt damping systems," *IEEE/ASME Trans. Mechatron.*, vol. 7, no. 1, pp. 87–94, Mar. 2002.
- [34] D. Niederberger, M. Morari, and S. Pietrzko, "Adaptive resonant shunted piezoelectric devices for vibration suppression," in *Proc. SPIE Smart Structures and Materials 2003: Damping and Isolation*, vol. 5052, San Diego, CA, Mar. 2003.
- [35] A. J. Fleming, S. Behrens, and S. O. R. Moheimani, "Synthetic impedance for implementation of piezoelectric shunt-damping circuits," *IEE Electron. Lett.*, vol. 36, no. 18, pp. 1525–1526, Aug. 2000.
- [36] C. C. Won, "Piezoelectric transformer," *J. Guid. Control Dyn.*, vol. 18, no. 1, pp. 96–101, 1995.
- [37] S. O. R. Moheimani, A. J. Fleming, and S. Behrens, "Dynamics, stability and control of multivariable piezoelectric shunts," *IEEE/ASME Trans. Mechatron.*, vol. 9, no. 1, pp. 87–99, Mar. 2004.
- [38] —, "On the feedback structure of wideband piezoelectric shunt damping systems," *IOP Smart Materials and Structures*, vol. 12, pp. 49–56, Jan. 2003.
- [39] L. Meirovitch, *Elements of Vibration Analysis*, 2nd ed. New York: McGraw-Hill, 1996.
- [40] A. R. Fraser and R. W. Daniel, *Perturbation Techniques for Flexible Manipulators*. Norwell, MA: Kluwer, 1991.
- [41] S. O. R. Moheimani, "Minimizing the effect of out-of-bandwidth dynamics in the models of reverberant systems that arise in modal analysis: Implications on spatial H_∞ control," *Automatica*, vol. 36, pp. 1023–1031, 2000.
- [42] S. Skogestad and I. Postlethwaite, *Multivariable Feedback Control*. New York: Wiley, 1996.
- [43] L. Ljung, *System Identification: Theory for the User*. Englewood Cliffs, NJ: Prentice-Hall, 1999.
- [44] T. McKelvey, H. Akcay, and L. Ljung, "Subspace based multivariable system identification from frequency response data," *IEEE Trans. Autom. Control*, vol. 41, no. 7, pp. 960–978, Jul. 1996.
- [45] R. Kalman, "When is a linear control system optimal," *J. Basic Eng.—Trans. ASME*, vol. 86, pp. 51–60, 1964.
- [46] M. G. Safonov and M. Athans, "Gain and phase margin for multiloop LQG regulators," *IEEE Trans. Autom. Control*, vol. AC-22, no. 2, pp. 173–179, Feb. 1977.
- [47] R. G. Brown and P. Hwang, *Introduction to Random Signals and Applied Kalman Filtering*. New York: Wiley, 1997.
- [48] J. C. Doyle, K. Glover, P. Khargonekar, and B. Francis, "State-space solutions to standard \mathcal{H}_2 and \mathcal{H}_∞ problems," *IEEE Trans. Autom. Control*, vol. 34, no. 8, pp. 831–847, Aug. 1989.
- [49] J. C. Doyle, B. A. Francis, and A. R. Tannenbaum, *Feedback Control Theory*. New York: Macmillan, 1992.
- [50] G. Zames, "Feedback and optimal sensitivity: Model reference transformations, multiplicative seminorms, and approximate inverse," *IEEE Trans. Autom. Control*, vol. AC-26, pp. 301–320, 1981.
- [51] C. K. Lee and F. C. Moon, "Modal sensors/actuators," *ASME J. Appl. Mech.*, vol. 57, pp. 434–441, Jun. 1990.
- [52] S. Behrens, S. O. R. Moheimani, and A. J. Fleming, "Multiple mode current flowing passive piezoelectric shunt controller," *J. Sound Vib.*, vol. 266, no. 5, pp. 929–942, Oct. 2003.
- [53] A. J. Fleming, "Synthesis and implementation of sensor-less shunt controllers for piezoelectric and electromagnetic vibration control." Ph.D. dissertation, The Univ. Newcastle, Callaghan, Australia, Feb. 2004.



Andrew J. Fleming (M'01) was born in Dingwall, Scotland, in 1977. He received the B.E. (Elec.) and Ph.D. degrees from The University of Newcastle, Callaghan, Australia, in 2000 and 2004, respectively.

His research involves nanopositioning, and sensor-less sound and vibration control.

Dr. Fleming is a member of the Center for Complex Dynamic Systems and Control, an Australian Government Special Research Centre.



S. O. Reza Moheimani (S'93–M'97–SM'00) received the B.Sc. degree from Shiraz University, Iran, in 1990 and the M.Eng.Sc. and Ph.D. degrees from the University of New South Wales, Australia in 1993 and 1996, respectively, all in electrical and electronics engineering.

In 1996, he was a Postdoctoral Research Fellow at the School of Electrical and Electronics Engineering, Australian Defence Force Academy, Canberra, Australia. In 1997, he joined the University of Newcastle, Australia where he is currently an Associate

Professor in the School of Electrical Engineering and Computer Science. He has over 100 journal and conference publications, is a co-author of the research monograph *Spatial Control of Vibration: Theory and Experiments* (Singapore: World Scientific, 2003) and the editor of the volume *Perspectives in Robust Control* (New York: Springer-Verlag, 2001).

Dr. Moheimani is an Associate Editor for IEEE TRANSACTIONS ON CONTROL SYSTEMS TECHNOLOGY, *Control Engineering Practice*, and *International Journal of Control, Automation, and Systems*. He has served on the editorial boards of several international conferences, and was the Chairman of International Program Committee for the 3rd IFAC Symposium on Mechatronic Systems, held in Sydney, Australia in 2004. His research interests include smart structures, mechatronic systems, control theory, and signal processing. He Moheimani is a member of the ARC Centre for Complex Dynamic Systems and Control, where he directs the Center's research in the area of mechatronics.